Low-Temperature Melt Processing of Organic−Inorganic Hybrid Films

David B. Mitzi,*,† David R. Medeiros,† and Patrick W. DeHaven‡

IBM T. J. Watson Research Center, P.O. Box 218, Yorktown Heights, New York 10598, and IBM Corporation, 2070, Route 52, Hopewell Junction, New York 12533

Received March 12, 2002
Revised Manuscript Received May 17, 2002

Organic−inorganic hybrids have generated substantial recent interest as a result of the ability to combine desirable organic and inorganic characteristics within a single molecular-scale composite as well as the possibility to evoke new properties from the interaction between the two components.[1] Hybrid perovskites, which consist of inorganic sheets of corner-sharing metal halide octahedra alternating with layers of organic ammonium cations, are one important hybrid family, exhibiting a number of interesting magnetic, optical, and electrical phenomena.[2,3] An electroluminescent dye-containing perovskite, for example, integrates the thermal/mechanical stability and band gap tunability of an inorganic framework with the desirable luminescence properties of an organic component.[4] Pronounced dips in the transmission spectrum of a perovskite-based photonic crystal slab result from the excitation of quasi-guided modes in the system.[5] An organic−inorganic thin-film transistor (OITFT) has also been demonstrated,[6,7] employing a $(C_6H_5C_2H_4NH_3)_2SnI_4$ perovskite as the channel semiconductor, with the organic−inorganic hybrid enabling the integration of simple processing associated with organic materials and higher carrier mobilities of inorganic semiconductors. Solution-processed hybrid OITFTs based on the tin(II) iodide framework have achieved saturation-regime mobilities ($\approx$1.0 $cm^2\ V^{-1}\ s^{-1}$) comparable to that of amorphous silicon.[7,8]

For electronic device applications as well as for many physical characterization techniques, the ability to conveniently deposit films is crucial. A number of techniques have been described for depositing hybrid films,[9] including multiple-source thermal evaporation,[10] single-source thermal ablation,[11] Langmuir−Blodgett,[12] two-step dip processing,[13] spin coating,[9] and stamping.[14] The solution-based processes are particularly attractive because they enable the quick and inexpensive deposition of the hybrids on a diverse array of substrates. Despite the convenience of solution processing, potential problems with solubility, surface wetting, and chemical incompatibility between the solvent and hybrid limit the application of these techniques. It is therefore essential to consider other possibilities for film processing, with a special emphasis on those techniques that are compatible with a range of substrate materials and shapes (of particular interest are flexible plastic substrates).

Melt processing has proven very useful for the processing of selected polymeric organic and inorganic materials and provides a natural opportunity to employ roll-to-roll, lamination, capillary-filling, and extrusion techniques.[15−18] Gradual heating of organic−inorganic hybrids might be expected to decompose or dissociate the organic component at a lower temperature than that required for melting. In the metal-halide-based perovskite family $(C_4H_9NH_3)_2MI_4$ (M = Pb, Sn, and Ge), however, the melting temperature progressively decreases across the series from Pb to Ge such that while both the M = Sn and Pb compounds decompose before or during melting (as is typical for the hybrids), the M = Ge compound forms a reasonably stable melt phase (T_m = 222 °C).[19] The present communication reports that the organic component of the perovskite can be used to lower the melting temperature of the hybrid well below the decomposition point ($T_m \lesssim$ 200 °C), thereby enabling melt processing of a wider range of organic−inorganic perovskites and the first demonstration of semiconducting melt-processed hybrid films on flexible plastic substrates. Temperature-dependent X-ray studies also demonstrate a structural transition before melting in these systems.

In an effort to examine the influence of the organic cation on the thermal properties of isostructural tin(II) iodide based hybrids, $(R{-}NH_3)_2SnI_4$, several related phenethylammonium-based cations were considered, including phenethylammonium (PEA), 2-fluorophenethylammonium (2-FPEA), 3-fluorophenethylammonium (3-FPEA), and 2,3,4,5,6-pentafluorophenethylam-

* To whom correspondence should be addressed.
† IBM T. J. Watson Research Center.
‡ IBM Corporation.

(1) See, for example, "Organic−Inorganic Nanocomposite Materials," special issue of *Chem. Mater.* **2001**, *13*, 3059−3809.
(2) For a recent review, see: Mitzi, D. B. *Prog. Inorg. Chem.* **1999**, *48*, 1.
(3) Mitzi, D. B.; Chondroudis, K.; Kagan, C. R. *IBM J. Res. Dev.* **2001**, *45*, 29.
(4) Chondroudis, K.; Mitzi, D. B. *Chem. Mater.* **1999**, *11*, 3028.
(5) Shimada, R.; Yablonskii, A. L.; Tikhodeev, S. G.; Ishihara, T. *IEEE Quantum Electron.* **2002**, in press.
(6) (a) Chondroudis, K.; Dimitrakopoulos, C. D.; Mitzi, D. B., unpublished work 1998. (b) Chondroudis, K.; Dimitrakopoulos, C. D.; Kagan, C. R.; Kymissis, I.; Mitzi, D. B. U.S. Patent US6180956, January 30, 2001.
(7) Kagan, C. R.; Mitzi, D. B.; Dimitrakopoulos, C. D. *Science* **1999**, *286*, 945.
(8) Mitzi, D. B.; Dimitrakopoulos, C. D.; Kosbar, L. L. *Chem. Mater.* **2001**, *13*, 3728.
(9) Mitzi, D. B. *Chem. Mater.* **2001**, *13*, 3283.
(10) Era, M.; Hattori, T.; Taira, T.; Tsutsui, T. *Chem. Mater.* **1997**, *9*, 8.
(11) Mitzi, D. B.; Prikas, M. T.; Chondroudis, K. *Chem. Mater.* **1999**, *11*, 542.
(12) Era, M.; Oka, S. *Thin Solid Films* **2000**, *376*, 232.
(13) Liang, K.; Mitzi, D. B.; Prikas, M. T. *Chem. Mater.* **1998**, *10*, 403.
(14) Kagan, C. R.; Breen, T. L.; Kosbar, L. L. *Appl. Phys. Lett.* **2001**, *79*, 3536.
(15) Wideman, T.; Sneddon, L. G. *Chem. Mater.* **1996**, *8*, 3.
(16) Miyagawa, K.; Tsunashima, K.; Sakamoto, Japan Patent JP2000202906, July 25, 2000.
(17) (a) Rabolt, J. F.; Clarke, T. C.; Kanazawa, K. K., Reynolds, J. R.; Street, G. B. *J. Chem. Soc., Chem. Commun.* **1980**, 347. (b) Chance, R. R.; Shacklette, L. W.; Miller, G. G.; Ivory, D. M.; Sowa, J. M.; Elsenbaumer, R. L.; Baughman, R. H. *J. Chem. Soc., Chem. Commun.* **1980**, 348.
(18) (a) Langhorn, J. B.; McGinn, P. J. *Physica C* **1999**, *323*, 79. (b) Holesinger, T. G.; Phillips, D. S.; Coulter, J. Y.; Willis, J. O.; Peterson, D. E. *Physica C* **1995**, *243*, 93.
(19) Mitzi, D. B. *Chem. Mater.* **1996**, *8*, 791.

10.1021/cm020264f CCC: $22.00
Published on Web 06/12/2002

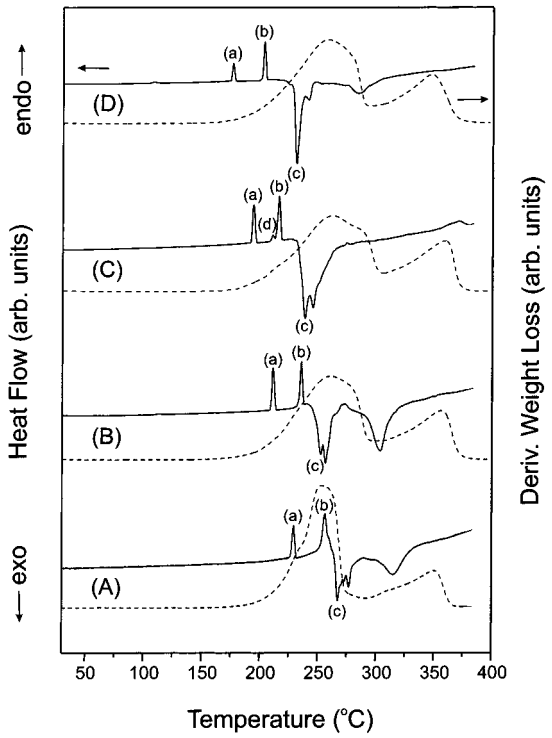

Figure 1. Derivative of the weight loss (dashed line) and heat flow (solid line) as a function of temperature for (A) $(5FPEA)_2SnI_4$, (B) $(3\text{-}FPEA)_2SnI_4$, (C) $(PEA)_2SnI_4$, and (D) $(2\text{-}FPEA)_2SnI_4$. The scans were performed in a flowing nitrogen atmosphere using ground crystals of each compound and a 2 °C/min ramp rate. The significant transitions are marked with (a), (b), and (c). The origins of these transitions are discussed in the text. A minor structural transition (d), which is only fully resolvable at slower ramp rates (<5 °C/min), is also noted in the $(PEA)_2SnI_4$ data before melting.

monium (5FPEA). The four perovskites were prepared as previously reported.[8,20] Figure 1 shows the thermogravimetric analysis (TGA) and differential scanning calorimetry (DSC) scans for each of the hybrids. In each system the peak rate of weight loss, corresponding to the dissociation or decomposition of the organic component, occurs at approximately the same temperature (255−261 °C). The second peak in weight loss, at ≈350 °C, primarily corresponds to the evolution of the SnI_2 component from the sample. Within the DSC scan, there are three major transitions marked (a)−(c). Visual examination of the hybrid crystals as they are gradually heated confirms that transition (b) corresponds to melting, while the hybrid perovskites undergo bulk decomposition at (c). As discussed below, transition (a) corresponds to a structural transition.

Importantly, despite the relative invariance of the temperature at which most of the organic component dissociates from the powdered samples and the similar tin(II) iodide framework, the temperatures of the structural transition (a) and the melting transition (b) progressively shift to lower temperature (Table 1) across the series $(R{-}NH_3)_2SnI_4$ (R = 5FPEA, 3-FPEA, PEA, and 2-FPEA). While the $(5FPEA)_2SnI_4$ sample decomposes as it melts, the melt becomes significantly more stable as the temperature of the melting transition (b), T_b, decreases across the cation series. Notably, the

(20) Mitzi, D. B.; Medeiros, D. R.; Malenfant, P. R. L. *Inorg. Chem.* **2002**, *41*, 2134.

Table 1. Transition Temperatures and Enthalpies for Transitions (a), (b), and (d)

	T_a (°C)	ΔH (a) (kJ/mol)	T_b (°C)	ΔH (b) (kJ/mol)	T_d (°C)	ΔH (d) (kJ/mol)
$(2\text{-}FPEA)_2SnI_4$	174.0(3)	11.9(2)	200.8(8)	26.7(5)		
$(PEA)_2SnI_4$	191.9(3)	18.5(4)	213.4(8)	23.9(6)[a]	208.2(5)	3.0(2)[a]
$(3\text{-}FPEA)_2SnI_4$	209.2(4)	24.3(5)	233.0(8)	25.8(5)		
$(5FPEA)_2SnI_4$	227.0(8)	19.1(4)	253(1)	39(1)[a]		

[a] Estimated value for overlapping transitions.

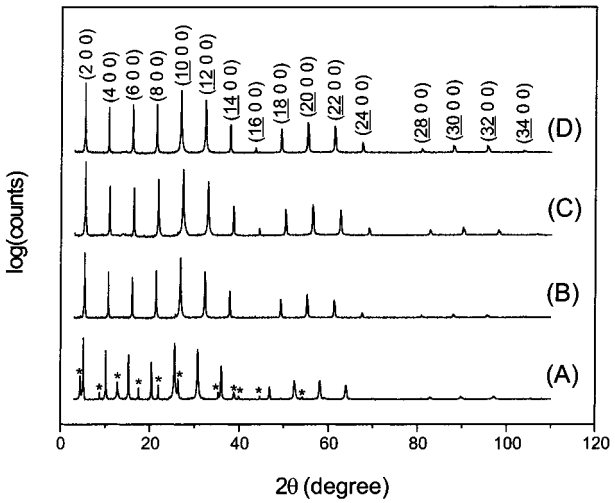

Figure 2. Room temperature X-ray diffraction patterns (Cu Kα radiation; $\lambda = 1.5418$ Å) for the laminated melt-processed films of (A) $(5FPEA)_2SnI_4$ [17.47(1) Å], (B) $(3\text{-}FPEA)_2SnI_4$ [16.63(1) Å], (C) $(PEA)_2SnI_4$ [16.31(1) Å], and (D) $(2\text{-}FPEA)_2SnI_4$ [16.64(1) Å], with the observed interlayer spacing between inorganic sheets noted in parentheses. The reflection indices are marked in (D) and the impurity peaks in pattern (A) (resulting from partial decomposition during melt processing) are noted using an *. The background signal from the Kapton was independently measured and subtracted from each pattern. Patterns (B)−(D) have been offset vertically for clarity.

temperatures of transitions (a) and (b) during thermal analysis are reproducible with respect to different heating rates, sample size, and morphology (crystal versus powder). In contrast, the decomposition temperature (c) appears to depend on how easy it is for the organic material to diffuse from the sample (i.e., for crystals, the transition is generally at a higher temperature than that for powders).

The ability to form a stable melt at low temperatures (≈200 °C) provides an ideal opportunity to process films of the semiconducting hybrids from the melt on organic-based substrates. In the present examples, the films are formed in a nitrogen-filled glovebox by heating (on a temperature-controlled hotplate) an 8-μm-thick Kapton sheet ≈10 °C above the expected melting temperature of the hybrid (Table 1), placing hybrid crystals or powder on the sheet and immediately depositing another Kapton sheet on top of the melting materials. The hybrid melt effectively wets the Kapton and capillary action spreads the melt uniformly between the sheets, leading to the formation of a film, the thickness of which depends on the initial quantity of hybrid (generally in the range 0.5−10 μm). Thinner hybrid films may be achieved by application of pressure to the top Kapton sheet during the melt process. After the film is allowed to spread, it is cooled below the melting temperature, resulting in a polycrystalline film laminated between the two Kapton sheets. The X-ray diffraction pattern

for the $(5FPEA)_2SnI_4$ sample (Figure 2A) indicates substantial decomposition during the melting process, while the $(3\text{-}FPEA)_2SnI_4$ sample (Figure 2B) has a slightly shifted spacing between the inorganic sheets relative to the bulk solution-grown crystals (16.63 vs 16.79 Å), presumably because of the proximity of the melting and decomposition transitions. The diffraction patterns for the two lower melting point films (Figure 2C,D), however, are identical to those of the initial crystals and the large number of higher order (*h* 0 0) reflections attest to the preferred orientation and high degree of crystallinity of the films. The resulting Kapton/hybrid/Kapton laminate is flexible and the Kapton sheets serve to partially protect the hybrid materials from the environment (as evidenced by repeated X-ray diffraction scans of the films in air). A higher degree of protection may be afforded by using Kapton sheets coated with a gas/moisture barrier layer.[21]

The *d* spacing for the (10 0 0) reflection for the melt-processed hybrid systems is shown in Figure 3 as a function of temperature. Clearly evident in this figure is the first-order structural transition at feature (a) of the DSC scans (Figure 1) and the disappearance of the diffraction pattern as the sample melts at (b). The structural transition involves a substantial lengthening of the *a* axis, presumably as a result primarily of a change in orientation/conformation of the organic component in the structure. Similar structural transitions have been noted in long-chain alkylammonium-based hybrid perovskites.[22,23] The influence of the organic cation on the melting/structural transition temperatures may derive from changes in the specific hydrogen-bonding interactions between the cation and the inorganic component of the structure, from different packing interactions (e.g., aromatic−aromatic interactions) among the organic cations, or more indirectly from subtle changes in the structure of the inorganic framework induced by the different cations.[8]

In summary, the organic cation component of the semiconducting tin(II) iodide based hybrid perovskites has been used to tailor the thermal properties (structural/melting transitions) of these systems such that the melting temperature is reduced well below that of SnI_2 (320 °C) as well as significantly below the decomposition temperature for both the hybrids and some prospective organic-based substrate materials. Consequently, melt-processed films have been prepared on Kapton sheets, providing a pathway for the fabrication of electronic devices (e.g., TFTs and LEDs) on flexible substrates. The melt-processing technique is also attractive as a result of the potential for use of roll-to-roll techniques to fabricate films and circuits as well as the ability to laminate the hybrid semiconductor between sheets of plastic, as a means of protecting the air-sensitive materials from the environment. Finally, optimization of the film grain structure through controlled cooling of the melted films should also be possible, thereby providing a means of improving material or device performance.

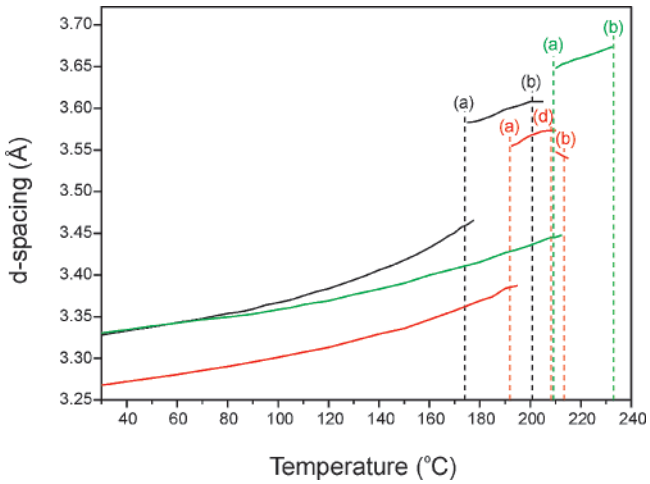

Figure 3. Lattice spacings for the (10 0 0) peak of melt-processed $(2\text{-}FPEA)_2SnI_4$ (black), $(PEA)_2SnI_4$ (red), and $(3\text{-}FPEA)_2SnI_4$ (green) films as a function of temperature, clearly demonstrating the structural transitions (a) and melting transitions (b). The films were measured using a Rigaku temperature-programmed diffractometer using Cr Kα radiation (λ = 2.2909 Å). For $(PEA)_2SnI_4$, a second structural transition (d) is resolved before melting, consistent with the DSC data (Figure 1). The vertical dashed lines mark the positions of transitions observed from thermal analysis data on bulk powder (Table 1), demonstrating good agreement among the structural/melting transition temperatures in bulk crystals and melt-processed films.

CM020264F

(21) See, for example, (a) Dennler, G.; Houdayer, A.; Ségui, Y.; Wertheimer, M. R. *J. Vac. Sci. Technol. A* **2001**, *19*, 2320. (b) Chatham, H. *Surf. Coat. Technol.* **1996**, *78*, 1.

(22) Needham, G. F.; Willett, R. D.; Franzen, H. F. *J. Phys. Chem.* **1984**, *88*, 674.

(23) Kammoun, S.; Kamoun, M.; Daoud, A.; Lautie, A. *J. Phys.: Condens. Matter* **1996**, *8*, 8465.